Decoding sub-seasonal drivers of extreme heat with interpretable machine learning

Jagger Alexander[1], Zong-Liang Yang[1]

[1]Jackson School of Geosciences, Department of Earth and Planetary Sciences, University of Texas at Austin, Austin, TX

Corresponding Author: Jagger Alexander (jaggeralexander@utexas.edu)

This is a non-peer-reviewed preprint uploaded to EarthArXiv. The manuscript is currently under submission to the American Meteorological Society's journal *Artificial Intelligence for the Earth Systems* (AIES).

Abstract

As climate change accelerates, heat waves are becoming more frequent, intense, and deadly. Enhancing predictive capabilities through a better understanding of sub-seasonal drivers of extreme heat is crucial for adaptation efforts. This study utilizes an interpretable machine learning model, implementing Extreme Gradient Boosting (XGBoost) with SHapley Additive exPlanations (SHAP), to evaluate the predictive strength of various climate factors—including local weather, global climate indices, geopotential heights, soil moisture, and sea surface temperatures—on extreme daily maximum temperatures. This model demonstrates strong predictive performance for extreme heat in Austin, TX, USA, on the sub-seasonal time scale, with soil moisture features emerging as more influential than atmospheric features. Notably, our analysis uncovers previously underexplored teleconnections between distant soil moisture anomalies and local extreme heat, warranting further investigation. It is also shown that the Madden-Julian Oscillation (MJO) has predictive value for extreme heat in Austin, underscoring its utility relative to other indices like ENSO and NAO. This method shows promise for application to other cities and for integration with dynamical modeling approaches, advancing sub-seasonal extreme heat forecasting more broadly.

Significance Statement

As heat waves intensify with climate change, there is an urgent need for more accurate sub-seasonal forecasts. This research presents a novel machine learning-based method to improve heat wave predictions, offering insights into key drivers of heat on the sub-seasonal scale and enabling earlier, more precise public health interventions that can reduce heat-related illness and mortality.

1. Introduction

Heat waves pose a significant and escalating threat to public health worldwide, with global trends demonstrating increases in their intensity, duration, seasonal length, and frequency due to anthropogenic climate change (Perkins-Kirkpatrick and Gibson 2017). The rate of heat wave occurrences has accelerated, resulting in a notable rise in heat-related mortality (Howard et al. 2024). However, forecasting heat waves, especially on sub-seasonal timescales (two weeks to two months) remains a challenge. While there are efforts using dynamical, statistical, machine-learning, and hybrid models for sub-seasonal forecasting efforts, their performance varies, and they are not currently operational for forecasting extreme heat events. Developing reliable methods to forecast these events with extended lead times is critical for enacting timely public health interventions.

This study introduces a novel machine-learning-based methodology to enhance sub-seasonal heat wave prediction. By extending the lead time and improving reliability of heat wave forecasts, this research aims to advance early warning systems and support public health strategies to mitigate the adverse effects of extreme heat.

Furthermore, this approach enables quantification and examination of the predictors and drivers of extreme heat on the sub-seasonal timescale, illuminating the specific interactions of various meteorological, land-surface, atmospheric, and ocean processes. This information will not only improve heat wave forecasting but also enhance broader understanding of sub-seasonal weather patterns, facilitating improvements in future models.

2. Related Work

Over the past decade, operational dynamical sub-seasonal forecasts have advanced significantly in skill, application, and utility (White et al. 2022), with the European Centre for Medium-Range Weather Forecasting (ECMWF) extended-range (up to 46 days) ensemble forecasts (Richardson et al. 2020) and the SubX Subseasonal Experiment (Pegion et al. 2019) among the leading efforts. While these models have successfully forecasted some extreme events (Vitart and Robertson 2018), other events have not been captured beyond three weeks lead time (Lin et al. 2022). The body of research on sub-seasonal extreme heat forecasting is still limited, restricting its operational use in emergency preparedness. Studies indicate that accurate sub-seasonal climate forecasting is the missing link in developing an early-warning system for heat-related mortality (Lowe et al. 2016), emphasizing that temperature-related illnesses are largely preventable with timely interventions.

Purely statistical or machine learning-based models for sub-seasonal forecasting of extreme heat have shown considerable skill, often matching or exceeding the performance of dynamical models (Miller et al. 2021; Weirich-Benet et al. 2023). Studies have identified dry soil moisture and persistent atmospheric blocking patterns as key factors for predicting extreme heat events (Wehrli et al. 2019; Lee et al. 2016; Zhang et al. 2023). Recently, hybrid models that integrate dynamical and machine-learning approaches, have demonstrated enhanced predictive skill compared to dynamical models alone (He et al. 2022; Chung et al. 2024; Hwang et al. 2019). However, further refinement in the selection of covariates and methodological approaches is needed to optimize the performance of these hybrid models.

Heat wave characteristics and drivers of heat waves vary by region and individual event (Wehrli et al. 2019; Jiang et al. 2023), underscoring the need for a thorough understanding of region-specific drivers to improve forecast accuracy. Austin, Texas, USA, is particularly vulnerable to the health effects of heat waves (Seong et al. 2023; Boumans et al. 2014), making it an ideal test case for this novel machine learning-based methodology. With drying summer soil moisture—a trend expected to persist (Nielsen-Gammon et al. 2020)—Austin's climate is shaped by complex land-atmosphere interactions, influences from the nearby Gulf of Mexico, and broader climate patterns originating from the Pacific, Atlantic, and Indian Oceans. Additionally, atmospheric blocking patterns contribute to the formation and persistence of heat waves in the region.

This study aims to assess the influence of these drivers through a machine-learning approach tailored to local heat wave prediction, leveraging a comprehensive range of variables. By examining the impact of these drivers, we aim to advance sub-seasonal heat wave forecasting in Austin and lay the groundwork for future regional hybrid models that integrate machine learning and dynamical approaches.

3. Data

Data for this study span the heat-wave season (June 1st through September 30th) for the 11-year period from 2013 through 2023. This period was chosen to ensure data availability for each of the predictive variables. Limiting the study to this period helps mitigate the confounding effects of vegetation change in Austin, TX and increased urbanization on heat wave prediction. Variables that change monotonically over the study period and/or vary too slowly would have insufficient training spaces for prediction and were therefore excluded from analysis, such as longer-term climate oscillations (e.g. Pacific Decadal Oscillation).

Climatological data were sourced from the NOAA NCEI Global Historical Climatology Network (GHCN) – Daily from the Austin Bergstrom International Airport (Station ID: USW00013958) (Menne et al., 2012). The climatological data for daily maximum temperatures were averaged for each day of the year over a 30-year period (1993 – 2022). Missing data (<1% of days) were excluded when averaging and calculating standard deviation. The standard deviation of daily maximum temperature was calculated for each day over the thirty-year period and used to create the 85th percentile threshold for defining heat-days. Both the mean and standard deviation were smoothed with a 2-week running average to reduce noise arising from natural variability.

The same Austin station provided daily weather data. These data contained fewer than 11 missing values over the study period (<1% of days), which were imputed with values from the nearest available date.

The Gulf of Mexico sea surface temperatures were obtained from the NOAA Optimum Interpolation Sea Surface Temperature (OISST) v2.1 dataset (Huang et al. 2021)—This gridded dataset incorporates buoy measurements, corrected by remotely sensed and ship data, and is interpolated to a 0.25° x 0.25° grid. The Gulf of Mexico region was defined by the grid cells within 20°N to 30°N latitude and 82°W to 95°W longitude. Daily sea surface temperatures (SSTs) across this area were averaged to produce a single daily mean SST value representing the Gulf of Mexico.

Global climate variability data were included to represent the state of the El Nino-Southern Oscillation (ENSO), the Madden-Julian Oscillation (MJO), and the North Atlantic Oscillation (NAO). First, the daily Southern Oscillation Index (SOI) from the Queensland Government's Long Paddock Centre was used, calculated as the pressure difference between Tahiti and Darwin relative to a 1933 – 1922 baseline (Queensland Government Dept. of Environment and Science 2019). Second, the Real-time Multivariate MJO (RMM) index, which characterizes the MJO through two values (RMM1 and RMM2), was used to represent the MJO's phase and amplitude. For clarity, the phase and amplitude values derived from this dataset were used instead of the raw RMM1 and RMM2 values (Wheeler and Hendon 2004). Finally, the daily NAO index sourced from NOAA/OAR/PSL (Boulder, Colorado, USA) and available from their website at https://psl.noaa.gov was used (Kalnay et al. 1996). This index compares 500 mb geopotential height anomalies to standard Northern Hemisphere loading patterns to produce a single NAO index value.

Atmospheric data were obtained from the ECMWF Reanalysis v5 (ERA5) hourly dataset (Hersbach et al. 2023), provided on a 31 km by 31 km grid and limited to the Western North

America region, spanning from 25°N to 55°N latitude and 90°W to 135°W longitude. Three pressure levels were analyzed, 850 mb (lower troposphere), 500 mb (mid-troposphere), and 250 mb (upper troposphere). For each pressure level, five metrics were derived: the latitudinal and longitudinal gradients of geopotential height across the Western North America region, the latitudinal and longitudinal gradients of geopotential height specific to Austin, Texas, and the geopotential height at Austin (30.25°N, 97.75°W). Gradients were calculated by converting latitude and longitude points to meter-based distances and computing the partial derivative of geopotential height in the north-south and east-west directions. This resulted in a total of fifteen values overall, five for each pressure level. Figure 1 provides an example of the 500 mb geopotential gradient variables for a single-timestep example.

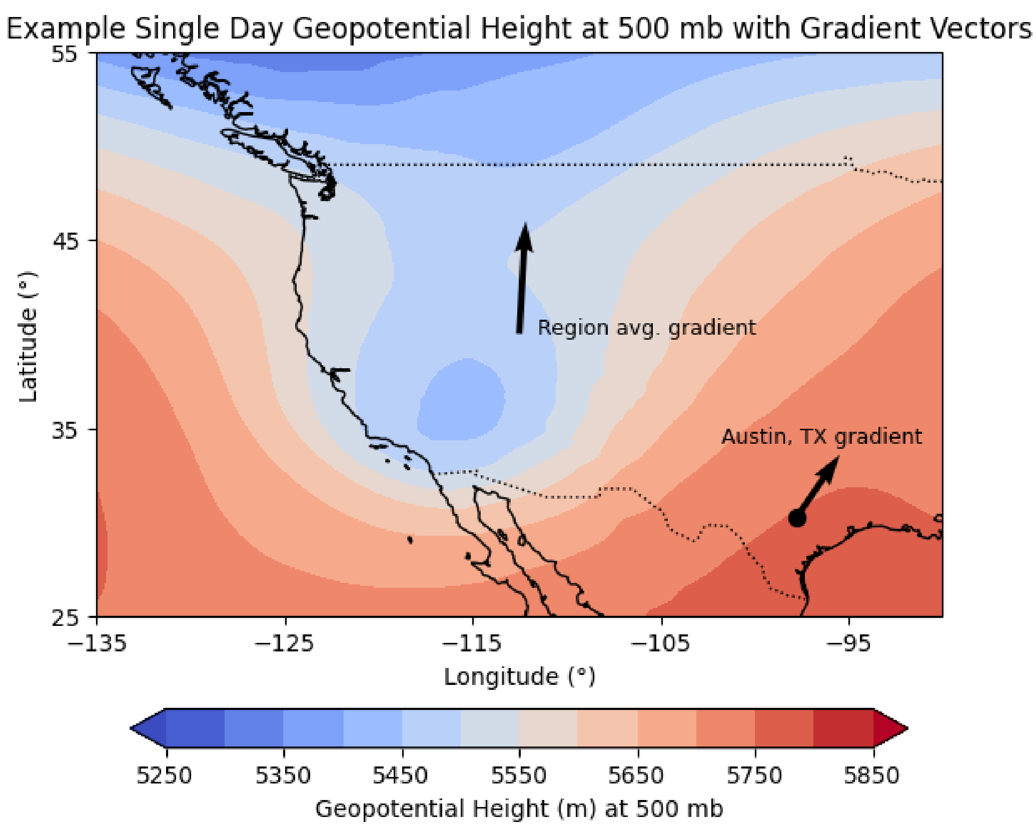

Figure 1. Example of 500 mb geopotential height on a single day, with vectors illustrating the average gradient across the Western North America region and the local gradient at Austin, Texas.

Finally, eighteen soil moisture values are included in the analysis, each representing one of the USGS-delineated hydrological regions across the United States (U.S. Geological Survey 2024). These values were generated by averaging the daily gridded soil moisture data from the Climate Prediction Center (CPC), which represent the soil moisture quantities within the top 1.6 meters of soil on an 0.25° x 0.25° grid (van den Dool et al. 2003), The GeoPandas package v1.0.1 (Jordahl et al. 2020) in Python v3.12.6 (Python Software Foundation 2023) was used to map each CPC soil moisture grid cell to its respective hydrological region. All grid cells within or intersecting a hydrological region were averaged to yield daily mean soil moisture for each hydrological region.

Prediction with multiple leads

Variables were classified as either "fast-changing" or "slow-changing." For fast-changing variables, three different leads were prescribed: the first representing the mean values of each daily variable from 21 to 23 days before the prediction, the second from 24 to 27 days, and the third from 28 to 34 days. For slow-changing variables, such as sea surface temperatures, certain global climate oscillations, and regional soil moisture, only one lead was used, representing the times from 21 to 34 days prior to the prediction. Only variables with leads were utilized for prediction, except for climatology, where values for the specific prediction day were provided. A full table of variables and their lead classification is shown below (Table 1).

<table>
<tr><th>Variable Name</th><th>Variable Type</th><th>Leads</th><th>Data Source</th></tr>
<tr><td>Max.Temp.</td><td rowspan="5">Meteorological</td><td rowspan="5">Fast-changing</td><td rowspan="7">NOAA NCEI GHCN
(Menne et al., 2012)</td></tr>
<tr><td>Min. Temp.</td></tr>
<tr><td>Relative Humidity</td></tr>
<tr><td>Avg. Wind Speed</td></tr>
<tr><td>Total Precip.</td></tr>
<tr><td>Normal Max. Temp.</td><td rowspan="2">Climatology</td><td rowspan="2">None</td></tr>
<tr><td>Normal Min. Temp.</td></tr>
<tr><td>SO Index</td><td>Global Climate Variability</td><td>Slow-changing</td><td>Daily SOI (Queensland Government Dept. of</td></tr>
</table>

			Environment and Science 2019)
NAO Index		Fast-changing	Daily NAO Index (Kalnay et al. 1996)
MJO Index (Amplitude & Phase)			Real-time Multivariate MJO Index (Wheeler and Hendon 2004)
Gulf of Mexico SST	Ocean	Slow-changing	NOAA OISST (Huang et al. 2021)
Lon. Grad. of W.N.A. 850 mb Geo. Height	Atmosphere	Fast-changing	ERA5 hourly single pressure level data (Hersbach et al. 2023)
Lat. Grad. of W.N.A. 850 mb Geo. Height			
Lon. Grad. of W.N.A. 500 mb Geo. Height			
Lat. Grad. of W.N.A. 500 mb Geo. Height			
Lon. Grad. of W.N.A. 250 mb Geo. Height			
Lat. Grad. of W.N.A. 250 mb Geo. Height			
Austin, TX 850 mb Geo. Height			
Austin, TX 500 mb Geo. Height			
Austin, TX 250 mb Geo. Height			
USGS Hydro. Unit-Averaged SM	Land Surface	Slow-changing	CPC Daily Soil Moisture (U.S. Geological Survey 2024)

Table 1. Variable name, type, leads, and data source for all daily predictive variables.

Heat wave identification

Heat wave days were identified by comparing daily maximum temperatures to the 85th percentile of the climatological maximum temperature. Specifically, a day was classified as a heat wave day if the three-day running average of daily maximum temperatures, centered on the current day, exceeded the 85th percentile of the smoothed climatology for that day. An example heat wave day classification is shown below for the summer of 2023 (Figure 1), where days are categorized as either heat wave days or non-heat wave days based on the climatological threshold. This definition allows flexibility. For instance, a single day with a maximum temperature significantly higher than climatology or three consecutive days with temperatures just over the 85th percentile both qualify as heat wave days.

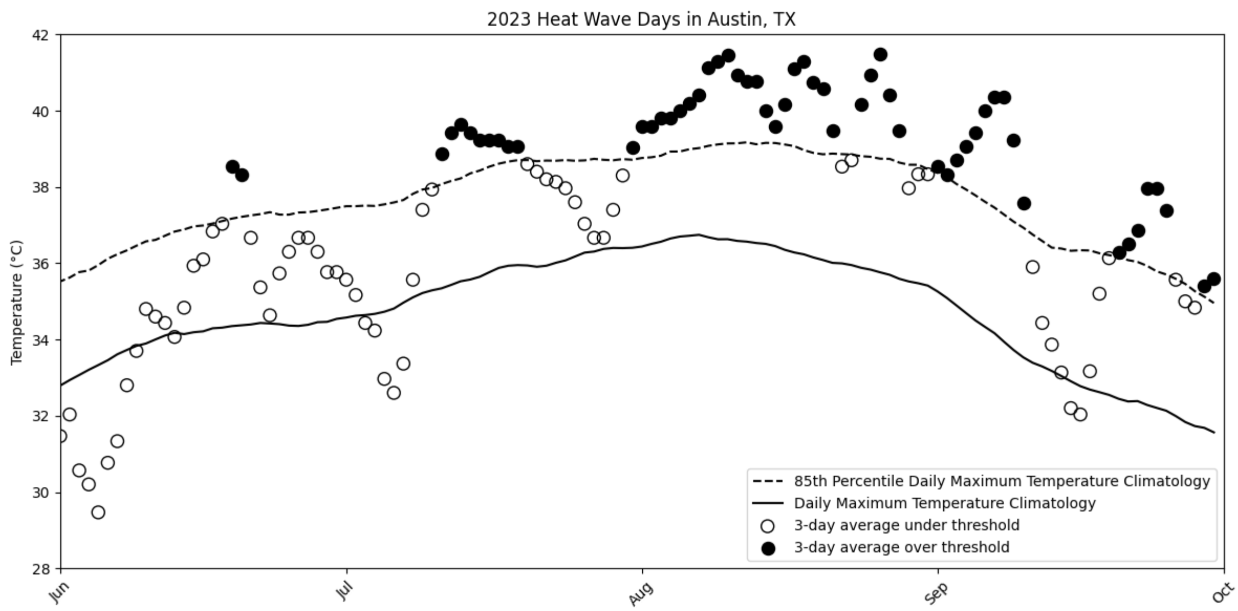

Figure 2. Heat wave identification in Austin, TX during 2023. Curves represent smoothed daily maximum temperature climatology using a two-week running average. Individual points represent 3-day average daily maximum temperatures.

	June	**July**	**August**	**September**	**Total**
2013	5	2	4	0	**11**
2017	0	3	0	0	**3**
2018	7	9	1	0	**17**
2019	0	0	0	8	**8**
2020	0	3	5	0	**8**
2021	0	0	0	1	**1**
2022	13	11	1	0	**25**
2023	2	10	26	18	**56**
Total	**27**	**38**	**37**	**27**	**129**

Table 2. Descriptive statistics of heat wave days in Austin, TX during the months of June through September of 2013 through 2023.

A total of 129 days met the criteria for a heat wave day over the months of June through September of 2013 through 2023. 37 of the days were in June, 38 were in July, 27 were in August, and 37 were in September. More than 40% of the days were in the summer of 2023, with 11 in 2013, 3 in 2017, 17 in 2018, 8 in 2019, 8 in 2020, 1 in 2021, and 25 in 2022.

4. Prediction & Interpretation

Machine learning models for heat wave-day classification were developed using eXtreme Gradient Boosting (XGBoost) (Chen and Guestrin 2016), chosen for its efficiency and high performance in handling diverse input variables in classification tasks. XGBoost models were run through Scikit-learn package v1.5.2 (Pedregosa et al. 2011) in Python v3.12.6. Each variable listed in Table 1 was used to predict whether a day meets the heat-wave day criteria in a binary classification task with logistic regression as the output function, evaluated by the log loss metric.

To ensure robust model performance without overfitting, four-fold validation was used. For this, the dataset was randomly divided into four subsets, each containing at least 25 heat wave days to ensure balance across folds. In each iteration, the model was trained on three of the four subsets and tested on the remaining subset. This process was repeated to create a single ensemble model with predictive guidance based on the mean outcomes from the validation folds. All models were created using common parameters. The learning rate, eta, was set to 0.1. The maximum tree depth was set to 4. The fraction of rows sampled by each tree was set to 0.8. The fraction of features sampled by each tree was also set to 0.8. The class imbalance weighting was calculated to be 11.3 and set accordingly.

The complete four-fold validation process was repeated ten times, producing an ensemble of models. Performance metrics, including accuracy, precision, recall, and F1 score were aggregated across all ensemble members to derive mean performance values.

To interpret the contributions of each feature in the machine learning model, Shapley Additive exPlanations (SHAP) values were utilized (Lundberg and Lee 2017). SHAP values quantify each variable’s impact on model output, providing a clear interpretation of feature influence on heat-wave day classification. These values are derived by evaluating the average marginal contribution of each feature to the model's predictions. By assigning an importance score to each feature based on its contribution, the relative predictive strength of features influencing heat-wave days at a sub-seasonal time scale can be quantified. SHAP values were averaged across the ten models in the ensemble to produce mean absolute SHAP scores for each feature, as well as ensemble-based partial dependence plots, which display SHAP values as a function of feature value.

After creating an initial XGBoost model that included all features, correlation analysis was conducted to ensure features were not highly collinear. Between variables with leads, there were thirty-three pairwise correlations such that $| r | > 0.8$. In these cases, the variable which had the higher SHAP score in the model inclusive of all variables was retained from each correlated pair and the other was excluded. This continued until no variables had a correlation $| r | > 0.8$. Ultimately, twenty features were excluded from the final refined model: four regional soil moisture features (Rio Grande Region, Upper Colorado Region, California Region, Arkansas-White-Red Region), two meteorological features (maximum temperature 21-day lead, maximum temperature 28-day lead), and fourteen atmospheric features (500 mb NA mean y-gradient 21-, 24-, and 28-day leads, 250 mb NA mean x-gradient 24- and 28-day leads, 500 mb NA mean x-gradient 28-day lead, 250 mb Austin geopotential height 21-, 24-, and 28-day leads, 500 mb Austin geopotential height 28-day lead, 500 mb y-gradient 21- and 28-day leads, 250 mb y-gradient 24- and 28-day leads). Full details on the SHAP scores of the initial model as well as the covariance matrix are provided in Supplemental Table 1 and Supplemental Figure 1.

A final case study of the 2023 heat wave season was performed. Each feature was averaged across 56 days during this season which met the heat wave day condition. The mean conditions for each feature were then inputted into the ensemble XGBoost prediction model. The resulting probability of a heat wave day for these conditions is then outputted by the model, and a SHAP explainer plot is generated showing the relative contribution of each feature to this prediction.

5. Results

The refined XGBoost ensemble model demonstrated strong predictive performance across several metrics. The mean accuracy across ensemble members was approximately 0.984, with recall, precision, and F1 score all exceeding 0.915 (Figure 2, Table 2). This indicates that the model was effective at identifying heat wave days while minimizing false positives and negatives.

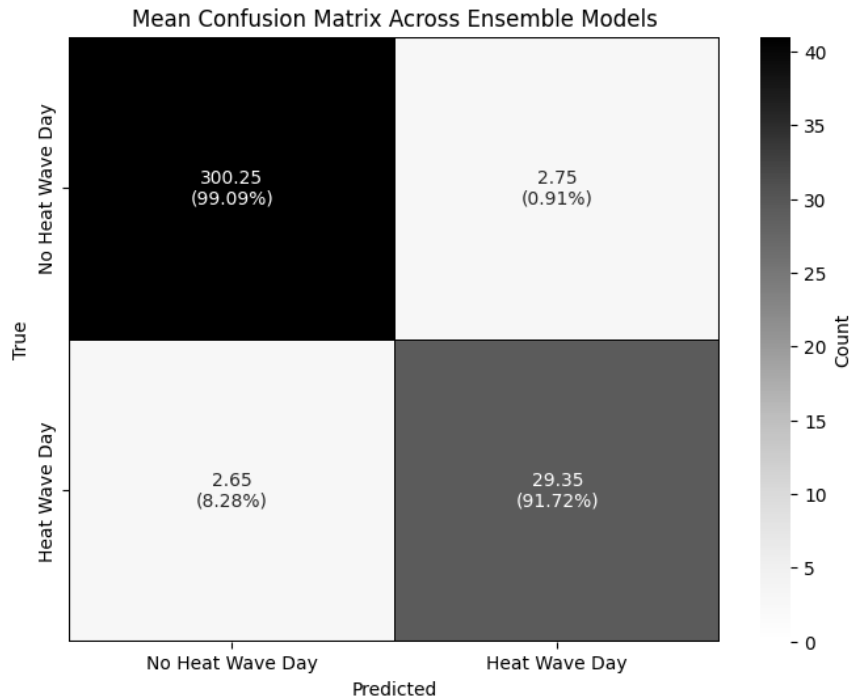

Figure 3. Mean confusion matrix of XGBoost model ensemble with refined feature selection.

Metric	**Mean**	**Standard Deviation**	**95% Confidence Interval**
Accuracy	0.984	0.002	(0.980, 0.988)
Recall	0.917	0.011	(0.895, 0.940)
Precision	0.915	0.012	(0.892, 0.938)
F1 Score	0.916	0.012	(0.893, 0.939)

Table 3. Performance metrics for XGBoost ensemble models using refined feature selection.

Among the predictors, the Texas-Gulf Region soil moisture stood out as the most influential feature (mean absolute SHAP value = 1.015), far exceeding the next strongest predictor, which had a mean absolute SHAP value of 0.432. Four of the top ten features were regional soil moisture values, including the Mid-Atlantic, New England, and Missouri regions. Relative humidity at 21- and 24-day leads were also strong predictors. Additionally, MJO amplitude at 28-day lead emerged as the fourth strongest feature. Geopotential height gradients, both longitudinal gradients at low to medium pressure levels (28- and 24-day leads, respectively) and latitudinal gradients at high pressure levels (21-day lead), were also among the top predictors.

As shown in Figure 3, predictors are divided into meteorological, atmospheric, and climate features for comparison. Notably, MJO amplitude and phase at 28-day lead time was a stronger predictor of heat wave days on the sub-seasonal time scale than the Gulf of Mexico SST, NAO at any lead, and SOI.

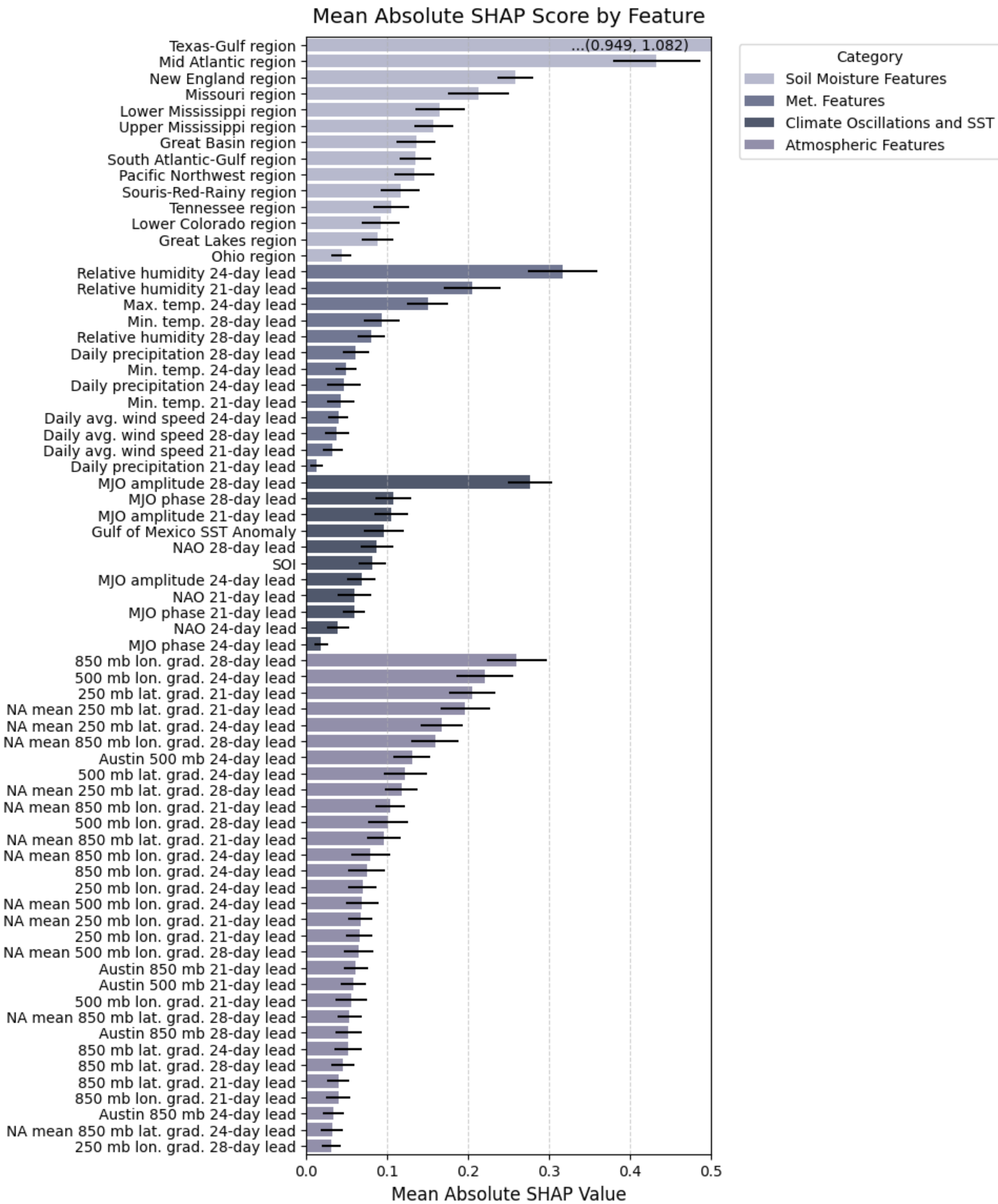

Figure 4. Mean absolute SHAP scores for land surface soil moisture, meteorological, atmospheric, and climate features.

Many regional soil moisture features demonstrated relatively high predictive power, as illustrated in Figure 4. Soil moisture values in distant regions, including the Mid-Atlantic and New England, were among the top predictors. Some nearby regions such as the Arkansas-White-Red region (omitted from refined model) did not show predictive skill.

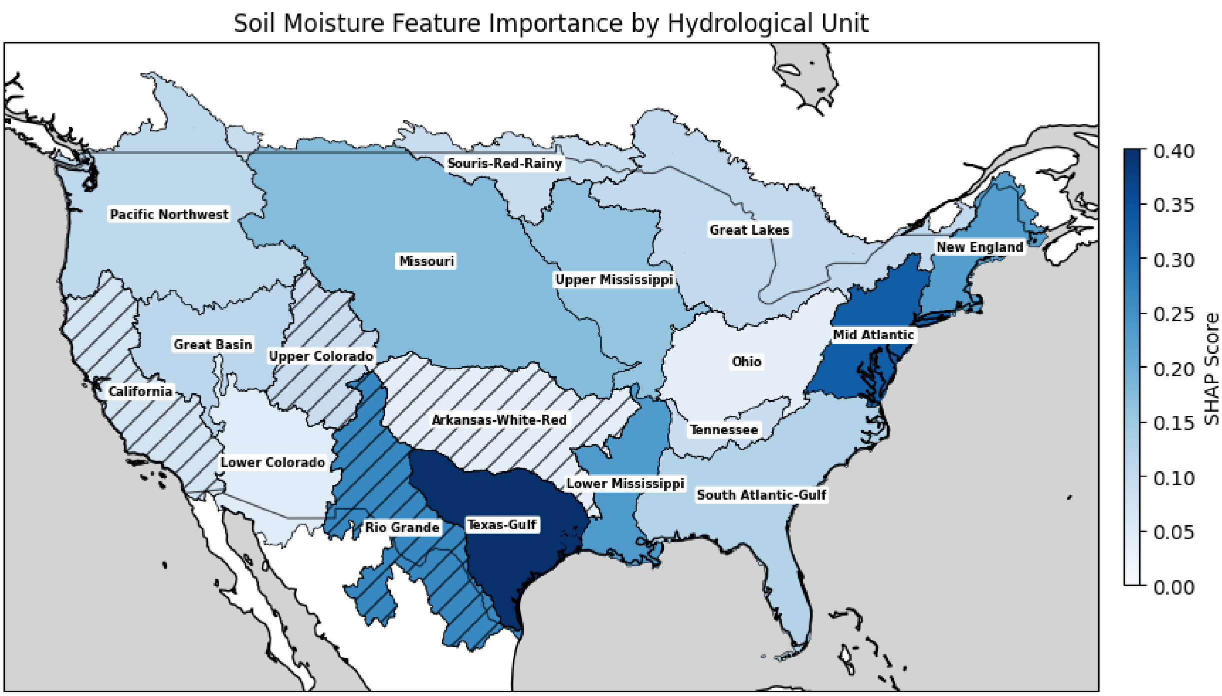

Figure 5. Map of soil moisture feature importance by means absolute SHAP score in initial unrefined ensemble model. Hatched regions were excluded in the refined ensemble model to reduce collinearity effects.

Figure 5 presents the partial dependence plots for the top five predictors in the model. The Texas-Gulf Region soil moisture had the strongest influence on heat wave prediction, with positive anomalies significantly reducing the likelihood of heat wave days. Conversely, the likelihood of a heat wave day increased with decreasing negative soil moisture anomalies. The Mid-Atlantic soil moisture exhibited a more complex relationship, but similarly, positive anomalies were associated with a lower chance of heat waves in Austin. The opposite trend is seen between New England soil moisture and Austin heat wave days. Lower relative humidity at a 24-day lead (below 70%) was more strongly correlated with heat waves, while higher values decreased this likelihood. High-amplitude MJO conditions (greater than 0.75) also reduced the probability of heat waves. Finally, stronger east-to-west 850 mb pressure gradients at a 28-day lead were linked to an increased likelihood of heat waves.

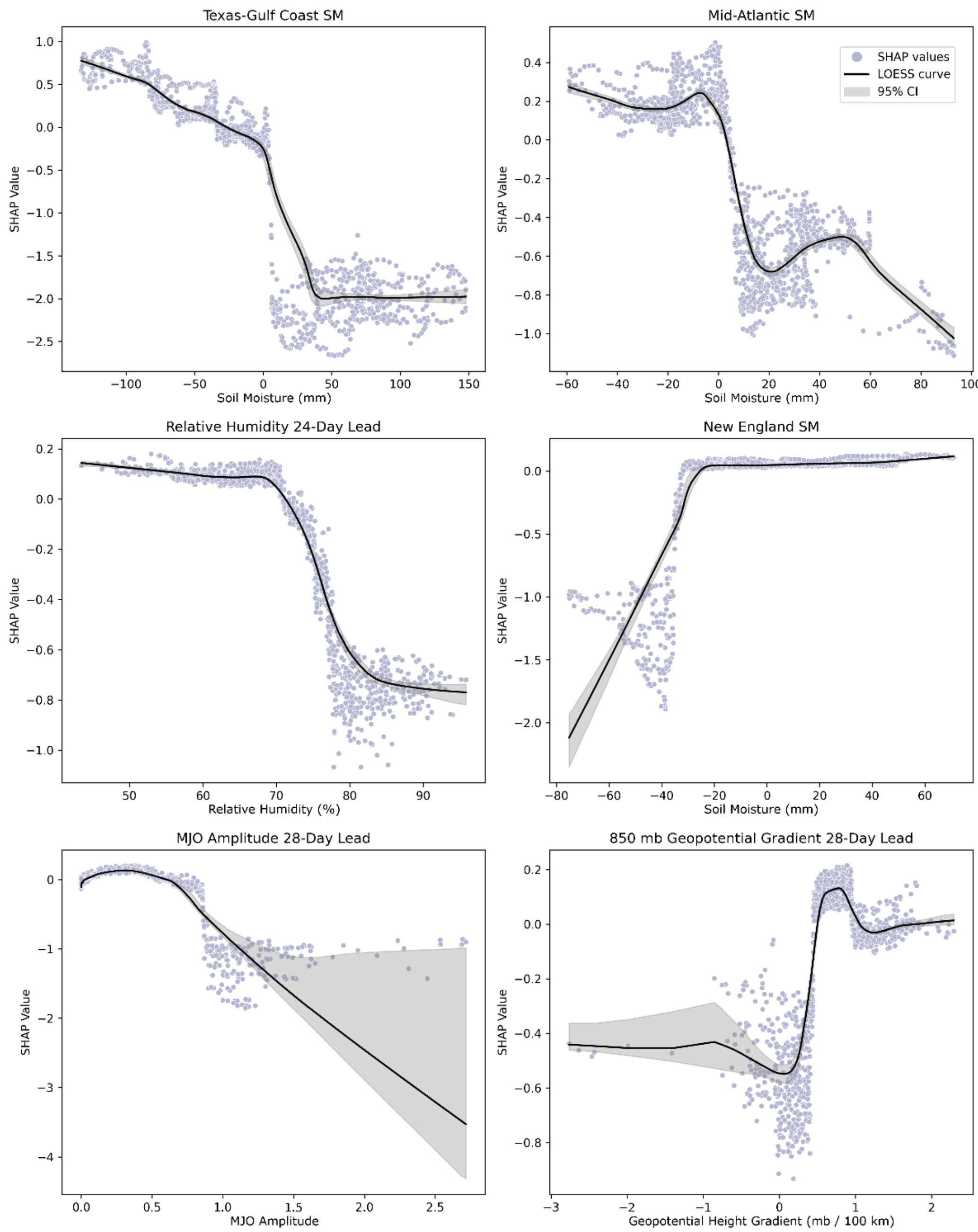

Figure 6. Partial dependence plots for the six features with the greatest mean absolute SHAP scores.

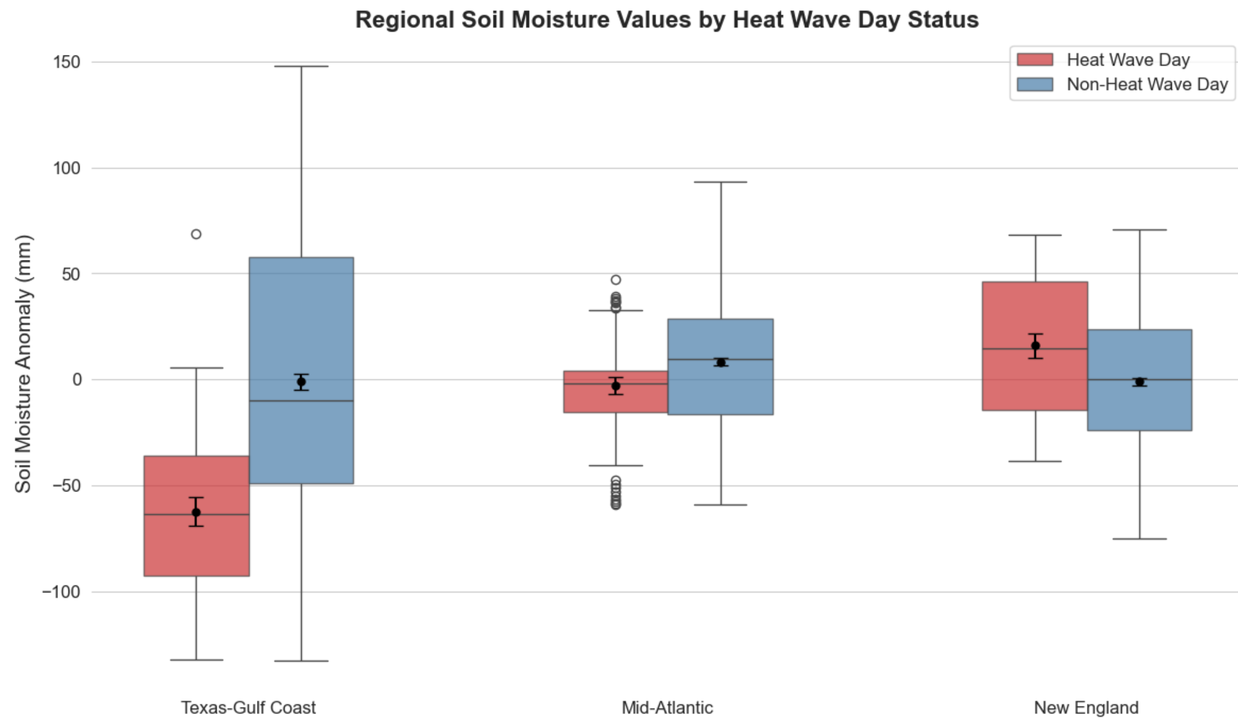

Figure 7. Box plot of soil moisture anomalies for heat wave day and non-heat wave day conditions for three strongest regional soil moisture features. Innermost black points and error bounds represent 95% confidence interval for the true mean.

Mean soil moisture anomalies were significantly lower on heat wave days compared to non-heat wave days in the Texas-Gulf Coast and Mid-Atlantic regions ($p < 0.05$) (Figure 7). In the Texas-Gulf Coast region, mean soil moisture anomalies were at least 50 mm lower during heat wave days than on non-heat wave days. Conversely, in the New England region, soil moisture anomalies were significantly higher on heat wave days than on non-heat wave days ($p < 0.05$).

The mean conditions during the 2023 heat wave resulted in the ensemble model predicting a 97.2% chance of a heat wave day, with a 95% confidence interval for the mean predicted probability of the ensemble members ranging from 96.6% to 97.9%. Figure 8 shows that regional soil moisture features primarily drive this prediction, with soil moisture conditions in Texas and neighboring regions, as well as more distant areas, counteracting upper tropospheric latitudinal geopotential height gradients in predicting heat wave days in Austin. In this figure, positive SHAP values (red) indicate contributions toward predicting heat wave days, while negative SHAP values suggest a prediction trend toward non-heat wave days.

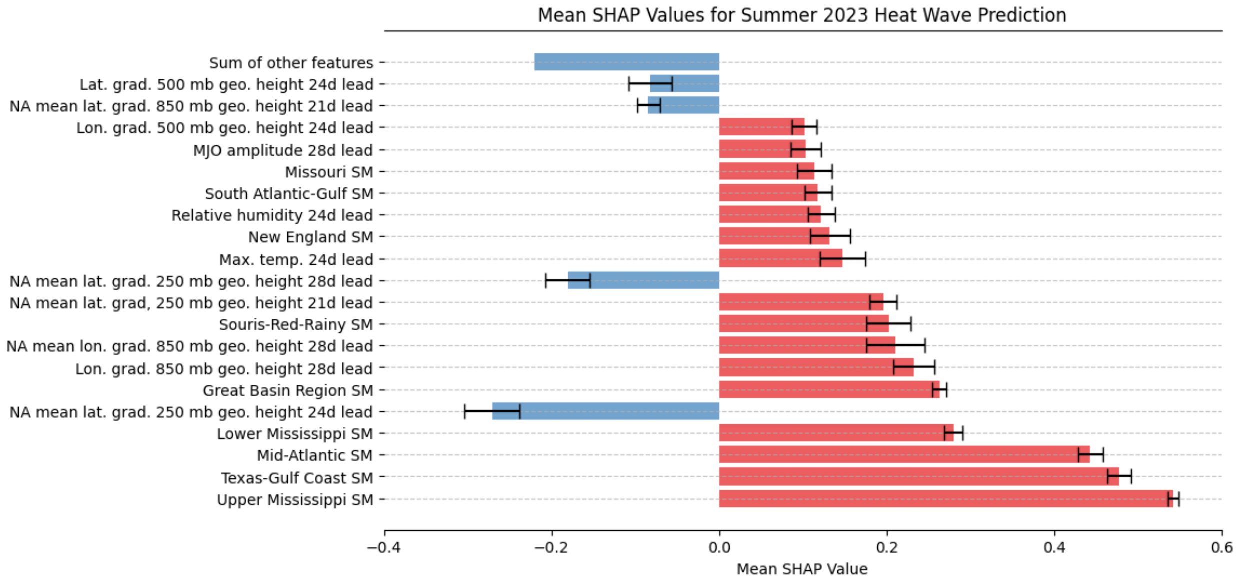

Figure 8. SHAP values derived from ensemble model predictions using mean 2023 heat wave day feature values. Error bars represent calculated 95% CI across the 10 ensemble model members.

Discussion

These results indicate that individual soil moisture features are the strongest predictors of sub-seasonal heat waves, with additional significant predictors spanning a variety of meteorological, atmospheric, and MJO indicators. Prior studies have similarly highlighted the influence of both atmospheric blocking patterns and land-surface characteristics on heat waves. However, this study finds that, at the sub-seasonal scale, local and teleconnected soil moisture features are generally more predictive of heat waves in Austin, Texas, than atmospheric factors alone (Wehrli et al. 2019). This finding aligns with other results which show soil moisture in Texas strongly correlating with temperature and heat waves specifically (Miralles et al. 2012).

The partial dependence plot for soil moisture in the Texas Gulf Coast region supports existing literature, showing that positive soil moisture anomalies are typically associated with a reduced likelihood of heat-wave days. Benson and Dirmeyer (2021) found a strong negative correlation ($r < -0.7$) between daily soil moisture and maximum temperature in the Texas-Gulf Coast region, though they note that the relationship is not linear and varies through different coupling regimes (weakly-coupled, sensitive, and hypersensitive). This study provides strong evidence that, below the mean soil moisture threshold, heat extremes are more likely, marking the transition between the sensitive and hypersensitive regimes in Austin, Texas. Dynamic modeling studies have shown that soil moisture conditions are particularly critical in heat wave modeling for regions situated between humid and arid climates (Seo et al. 2019), which supports the importance of local soil moisture in predicting Texas heat waves.

The predictive relationship between soil moisture in distant regions and heat waves in Texas has significant physical implications. This relationship, shown in this study by the strong mean absolute SHAP scores in the general XGBoost model and strengthened by similarly strong feature importances in the 2023 heat wave case study, shows that while some atmospheric features predicted against the likelihood of a heat wave, teleconnected soil moisture features countered these atmospheric features in accurately predicting a heat wave with the conditions prescribed. Sub-seasonal planetary wave patterns, commonly associated with heat waves (Barriopedro et al. 2023; Teng et al. 2013)—especially those with wavenumbers 5 through 8—may drive or be driven by teleconnections between soil moisture anomalies and extreme heat events across different areas. For instance, Li et al. (2024) suggest a mechanism for the 2021 Pacific Northwest Heat Dome, where decreased soil moisture induced a high-pressure ridge, ultimately leading to quasi-resonant amplification of planetary waves and a stationary high-pressure ridge. In such cases, soil moisture anomalies in one region may influence the ridge-trough pattern of Rossby waves, affecting the likelihood of extreme temperatures in Texas. Other studies have noted that heat waves often co-occur within spatially networked regions across CONUS (Mondal and Mishra 2021) and other global regions (Miloshevich et al. 2023), potentially linking these patterns to cross-regional soil moisture correlations. Future research should investigate the co-occurrence of heat waves in the Mid-Atlantic, New England, and Texas Gulf Coast regions, focusing on soil moisture effects using coupled Land Surface Models and GCMs.

The MJO was found to be a stronger predictor of heat waves over Texas than ENSO or NAO on the sub-seasonal time scale. Lower MJO amplitude at a longer lead time (28 to 34 days) was more strongly associated with heat waves over Austin. Other studies have shown summertime temperatures and heat waves over CONUS associated with MJO (Lee and Grotjahn 2019; Krishnamurthy et al. 2021). While the relationship between phase and amplitude at various lead-times on extreme heat is difficult to decode in this study, future work should investigate different MJO definitions to maximize predictability on heat waves over Austin.

Atmospheric features, though shown in this study and others (Adams et al. 2021) to be significant predictors of heat waves, are also complex to interpret. These results show that stronger east-to-west low-level geopotential gradients at 28- to 34-day lead time are more likely to result in heat wave formation in the US. However, combinations of different atmospheric variables are not easily interpretable. Different methodologies for simplifying complex multi-level atmospheric information into a series of interpretable variables should be investigated to better understand the value of local and global atmospheric trends on heat-wave predictability.

Though this model shows strong skill with similar amounts of false positives and negatives, for operational purposes, this method can intentionally be modified to minimize false negatives, erring on the side of over-predicting heat waves rather than missing true heat waves in prediction. However, it should be emphasized that the model will be tested in live-time and likely amended with dynamical model data and other covariates before being recommended for any operational use.

6. Conclusions

The ensemble model's strong performance in predicting heat wave days underscores its potential as an effective tool for sub-seasonal heat wave forecasting in Austin. This study serves as a significant foundation for regional hybrid models that leverage both machine-learning and dynamical approaches, providing a promising pathway for localized heat-health impact systems. With further refinement, this approach could offer critical advancements for public health preparedness, particularly in urban settings facing increased heatwave risk. Future studies that test regional differences will support a broader understanding of heat-wave formation on the sub-seasonal time scale, providing information on how predictors vary in regions with different climatic background conditions.

Future work will test these predictions in real-time and update the model with new training sets. Heat-wave dynamics will likely change as the climate changes, changing the trends and relative importance and of predictors. The model's flexible framework and high interpretability make it a strong and usable option for developing early-warning heat-health impact predictions, serving as a prototype for future guiding models on the health impacts of extreme heat.

Acknowledgements

J.J.A. acknowledges the University of Texas at Austin, Jackson School of Geosciences, Department of Earth and Planetary Sciences, for support through a Graduate Fellowship, Graduate Teaching Assistantship, and Independent Study Semester Fellowship. Additionally, we extend our gratitude to Kerry H. Cook, Geeta G. Persad, and Catherine Cubbin for their valuable insights, which helped guide this study.

Availability Statement

All data used for analyses in this study are publicly accessible through their original web access point. Weather and climatological data are available at www.ncei.noaa.gov/access. Soil moisture data are available at www.cpc.ncep.noaa.gov/products/Soilmst_Monitoring. SOI data are available at www.data.qld.gov.aus/dataset/the-southern-oscillation-index-daily. NAO data are available at www.cpc.ncep.noaa.gov/products/precip/CWlink/pna/NAO.shtml. MJO data are available at iridl.ldeo.columbia.edu/SOURCES/.BoM/.MJO/.RMM. Hydrological region data are available at www.usgs.gov/national-hydrography/watershed-boundary-dataset. Atmospheric reanalysis data are available at cds.climate.copernicus.eu/datasets. Sea surface temperatures data are available at www.ncei.noaa.gov/products/optimum-interpolation-sst.

References

Adams, R. E., C. C. Lee, E. T. Smith, and S. C. Sheridan, 2021: The relationship between atmospheric circulation patterns and extreme temperature events in North America. *International Journal of Climatology*, **41**, 92–103, https://doi.org/10.1002/joc.6610.

Barriopedro, D., R. García-Herrera, C. Ordóñez, D. G. Miralles, and S. Salcedo-Sanz, 2023: Heat Waves: Physical Understanding and Scientific Challenges. *Reviews of Geophysics*, **61**, e2022RG000780, https://doi.org/10.1029/2022RG000780.

Benson, D. O., and P. A. Dirmeyer, 2021: Characterizing the Relationship between Temperature and Soil Moisture Extremes and Their Role in the Exacerbation of Heat Waves over the Contiguous United States. https://doi.org/10.1175/JCLI-D-20-0440.1.

Boumans, R. J. M., D. L. Phillips, W. Victery, and T. D. Fontaine, 2014: Developing a model for effects of climate change on human health and health–environment interactions: Heat stress in Austin, Texas. *Urban Climate*, **8**, 78–99, https://doi.org/10.1016/j.uclim.2014.03.001.

Chen, T., and C. Guestrin, 2016: XGBoost: A Scalable Tree Boosting System. *Proceedings of the 22nd ACM SIGKDD International Conference on Knowledge Discovery and Data Mining*, *KDD '16*, New York, NY, USA, Association for Computing Machinery, 785–794.

Chung, U., J. Rhee, M. Kim, and S.-J. Sohn, 2024: Advancing sub-seasonal to seasonal multi-model ensemble precipitation prediction in east asia: Deep learning-based post-processing for improved accuracy. *Heliyon*, **10**, https://doi.org/10.1016/j.heliyon.2024.e35933.

van den Dool, H., J. Huang, and Y. Fan, 2003: Performance and analysis of the constructed analogue method applied to U.S. soil moisture over 1981–2001. *Journal of Geophysical Research: Atmospheres*, **108**, https://doi.org/10.1029/2002JD003114.

He, S., X. Li, L. Trenary, B. A. Cash, T. DelSole, and A. Banerjee, 2022: Learning and Dynamical Models for Sub-seasonal Climate Forecasting: Comparison and Collaboration. *AAAI*, **36**, 4495–4503, https://doi.org/10.1609/aaai.v36i4.20372.

Hersbach, H., and Coauthors, 2023: ERA5 hourly data on single levels from 1940 to present. https://doi.org/10.24381/CDS.ADBB2D47.

Howard, J. T., N. Androne, K. C. Alcover, and A. R. Santos-Lozada, 2024: Trends of Heat-Related Deaths in the US, 1999-2023. *JAMA*, **332**, https://doi.org/10.1001/jama.2024.16862.

Huang, B., C. Liu, V. Banzon, E. Freeman, G. Graham, B. Hankins, T. Smith, and H.-M. Zhang, 2021: Improvements of the Daily Optimum Interpolation Sea Surface Temperature (DOISST) Version 2.1. *Journal of Climate*, **34**, 2923–2939, https://doi.org/10.1175/JCLI-D-20-0166.1.

Hwang, J., P. Orenstein, J. Cohen, K. Pfeiffer, and L. Mackey, 2019: Improving Subseasonal Forecasting in the Western U.S. with Machine Learning. *Proceedings of the 25th ACM SIGKDD International Conference on Knowledge Discovery & Data Mining, KDD '19*, New York, NY, USA, Association for Computing Machinery, 2325–2335.

Jiang, L., J. Zhang, Q. Liu, X. Meng, L. Shi, D. Zhang, and M. Xing, 2023: Spatiotemporal variations of the global compound heat wave and the drivers of its spatial heterogeneity. *Journal of Cleaner Production*, **408**, 137201, https://doi.org/10.1016/j.jclepro.2023.137201.

Jordahl, K., and Coauthors, 2020: GeoPandas. https://doi.org/10.5281/zenodo.3946761.

Kalnay, E., and Coauthors, 1996: The NCEP/NCAR 40-Year Reanalysis Project.

Krishnamurthy, V., and Coauthors, 2021: Sources of Subseasonal Predictability over CONUS during Boreal Summer. https://doi.org/10.1175/JCLI-D-20-0586.1.

Lee, E., R. Bieda, J. Shanmugasundaram, and H. Basara Richter, 2016: Land surface and atmospheric conditions associated with heat waves over the Chickasaw Nation in the South Central United States. *Journal of Geophysical Research: Atmospheres*, **121**, 6284–6298, https://doi.org/10.1002/2015JD024659.

Lee, Y.-Y., and R. Grotjahn, 2019: Evidence of Specific MJO Phase Occurrence with Summertime California Central Valley Extreme Hot Weather. *Adv. Atmos. Sci.*, **36**, 589–602, https://doi.org/10.1007/s00376-019-8167-1.

Li, X., M. E. Mann, M. F. Wehner, S. Rahmstorf, S. Petri, S. Christiansen, and J. Carrillo, 2024: Role of atmospheric resonance and land–atmosphere feedbacks as a precursor to the June 2021 Pacific Northwest Heat Dome event. *Proceedings of the National Academy of Sciences*, **121**, e2315330121, https://doi.org/10.1073/pnas.2315330121.

Lin, H., R. Mo, and F. Vitart, 2022: The 2021 Western North American Heatwave and Its Subseasonal Predictions. *Geophysical Research Letters*, **49**, e2021GL097036, https://doi.org/10.1029/2021GL097036.

Lowe, R., M. García-Díez, J. Ballester, J. Creswick, J.-M. Robine, F. R. Herrmann, and X. Rodó, 2016: Evaluation of an Early-Warning System for Heat Wave-Related Mortality in Europe: Implications for Sub-seasonal to Seasonal Forecasting and Climate Services. *International Journal of Environmental Research and Public Health*, **13**, 206, https://doi.org/10.3390/ijerph13020206.

Lundberg, S. M., and S.-I. Lee, 2017: A Unified Approach to Interpreting Model Predictions. *Advances in Neural Information Processing Systems*, Vol. 30 of, Curran Associates, Inc. https://papers.nips.cc/paper_files/paper/2017/hash/8a20a8621978632d76c43dfd28b67767-Abstract.html (Accessed November 1, 2024).

Menne, M. J., I. Durre, R. S. Vose, B. E. Gleason, and T. G. Houston, 2012: An Overview of the Global Historical Climatology Network-Daily Database. https://doi.org/10.1175/JTECH-D-11-00103.1.

——, and Coauthors, Global Historical Climatology Network - Daily (GHCN-Daily). https://doi.org/10.7289/V5D21VHZ.

Miller, D. E., Z. Wang, B. Li, D. S. Harnos, and T. Ford, 2021: Skillful Subseasonal Prediction of U.S. Extreme Warm Days and Standardized Precipitation Index in Boreal Summer. https://doi.org/10.1175/JCLI-D-20-0878.1.

Miloshevich, G., P. Rouby-Poizat, F. Ragone, and F. Bouchet, 2023: Robust intra-model teleconnection patterns for extreme heatwaves. *Front. Earth Sci.*, **11**, https://doi.org/10.3389/feart.2023.1235579.

Miralles, D. G., M. J. van den Berg, A. J. Teuling, and R. a. M. de Jeu, 2012: Soil moisture-temperature coupling: A multiscale observational analysis. *Geophysical Research Letters*, **39**, https://doi.org/10.1029/2012GL053703.

Mondal, S., and A. K. Mishra, 2021: Complex Networks Reveal Heatwave Patterns and Propagations Over the USA. *Geophysical Research Letters*, **48**, e2020GL090411, https://doi.org/10.1029/2020GL090411.

Nielsen-Gammon, J. W., and Coauthors, 2020: Unprecedented Drought Challenges for Texas Water Resources in a Changing Climate: What Do Researchers and Stakeholders Need to Know? *Earth's Future*, **8**, e2020EF001552, https://doi.org/10.1029/2020EF001552.

Pedregosa, F., and Coauthors, 2011: Scikit-learn: Machine Learning in Python. *J. Mach. Learn. Res.*, **12**, 2825–2830.

Pegion, K., and Coauthors, 2019: The Subseasonal Experiment (SubX): A Multimodel Subseasonal Prediction Experiment. https://doi.org/10.1175/BAMS-D-18-0270.1.

Perkins-Kirkpatrick, S. E., and P. B. Gibson, 2017: Changes in regional heatwave characteristics as a function of increasing global temperature. *Sci Rep*, **7**, 12256, https://doi.org/10.1038/s41598-017-12520-2.

Python Software Foundation, 2023: Python 3.12.6.

Queensland Government Dept. of Environment and Science, 2019: Daily Southern Oscillation Index (SOI) Data (1933-1992 Base). https://www.longpaddock.qld.gov.au/soi/soi-data-files/ (Accessed September 23, 2024).

Richardson, D., H. Cloke, and F. Pappenberger, 2020: Evaluation of the Consistency of ECMWF Ensemble Forecasts. *Geophysical Research Letters*, **47**, https://doi.org/10.1029/2020GL087934.

Seo, E., and Coauthors, 2019: Impact of soil moisture initialization on boreal summer subseasonal forecasts: mid-latitude surface air temperature and heat wave events. *Clim Dyn*, **52**, 1695–1709, https://doi.org/10.1007/s00382-018-4221-4.

Seong, K., J. Jiao, and A. Mandalapu, 2023: Evaluating the effects of heat vulnerability on heat-related emergency medical service incidents: Lessons from Austin, Texas. *Environment and Planning B: Urban Analytics and City Science*, **50**, 776–795, https://doi.org/10.1177/23998083221129618.

Teng, H., G. Branstator, H. Wang, G. A. Meehl, and W. M. Washington, 2013: Probability of US heat waves affected by a subseasonal planetary wave pattern. *Nature Geosci*, **6**, 1056–1061, https://doi.org/10.1038/ngeo1988.

U.S. Geological Survey, 2024: Hydrological Unit Boundaries for the United States, Puerto Rico, and the U.S. Virgin Islands. https://doi.org/10.5066/P9MYEDA7.

Vitart, F., and A. W. Robertson, 2018: The sub-seasonal to seasonal prediction project (S2S) and the prediction of extreme events. *npj Clim Atmos Sci*, **1**, 1–7, https://doi.org/10.1038/s41612-018-0013-0.

Wehrli, K., B. Guillod, M. Hauser, M. Leclair, and S. Seneviratne, 2019: Identifying Key Driving Processes of Major Recent Heat Waves. *Journal of Geophysical Research: Atmospheres*,.

Weirich-Benet, E., M. Pyrina, B. Jiménez-Esteve, E. Fraenkel, J. Cohen, and D. I. V. Domeisen, 2023: Subseasonal Prediction of Central European Summer Heatwaves with Linear and Random Forest Machine Learning Models. https://doi.org/10.1175/AIES-D-22-0038.1.

Wheeler, M. C., and H. H. Hendon, 2004: An All-Season Real-Time Multivariate MJO Index: Development of an Index for Monitoring and Prediction. *Monthly Weather Review*, **132**, 1917–1932, https://doi.org/10.1175/1520-0493(2004)132<1917:AARMMI>2.0.CO;2.

White, C. J., and Coauthors, 2022: Advances in the Application and Utility of Subseasonal-to-Seasonal Predictions. https://doi.org/10.1175/BAMS-D-20-0224.1.

Zhang, X., and Coauthors, 2023: Increased impact of heat domes on 2021-like heat extremes in North America under global warming. *Nat Commun*, **14**, 1690, https://doi.org/10.1038/s41467-023-37309-y.

Supplemental Materials

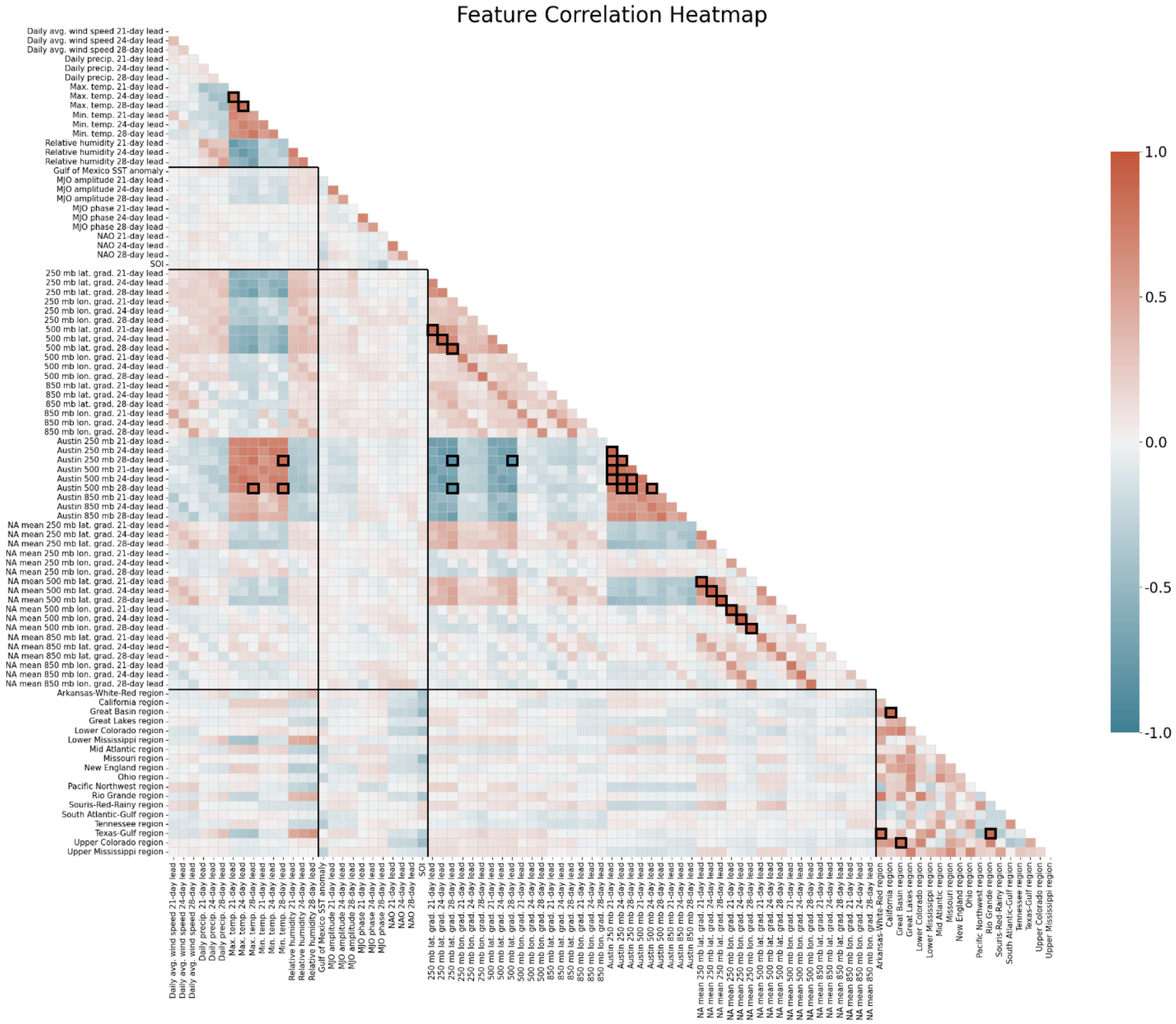

Supplemental Figure 1. Linear correlation for all predictive variables with leads. Correlations with |r| > 0.8 are displayed with a dark black border.

Feature	Mean Absolute SHAP Value
Texas-Gulf region	0.792585
Mid-Atlantic region	0.328136
Relative humidity 24-day lead	0.296123
Rio Grande region	0.265358
MJO amplitude 28-day lead	0.250870

Lower Mississippi region	0.235458
New England region	0.228183
850 mb geo. height lon. grad. 28-day lead	0.221595
500 mb geo. height lon. grad. 24-day lead	0.210387
250 mb geo. height lat. grad. 21-day lead	0.176403
Missouri region	0.173935
Upper Mississippi region	0.159643
Relative humidity 21-day lead	0.151433
NA mean 250 mb geo. height lat. grad. 21-day lead	0.143922
250 mb geo. height lat. grad. 28-day lead	0.135279
Max. temp. 24-day lead	0.134719
NA mean 850 mb geo. height lon. grad. 28-day lead	0.129531
South Atlantic-Gulf region	0.123480
Great Basin region	0.113655
Austin 500 mb 24-day lead	0.111889
Pacific Northwest region	0.109545
NA mean 850 mb geo. height lon. grad. 21-day lead	0.105724
MJO amplitude 21-day lead	0.104921
Great Lakes region	0.103755
NA mean 250 mb geo. height lat. grad. 24-day lead	0.102857
Austin 250 mb 24-day lead	0.102441
MJO phase 28-day lead	0.095682
Souris-Red-Rainy region	0.093903
Upper Colorado region	0.092679
Max. temp. 21-day lead	0.091233
Tennessee region	0.090233
NA mean 850 mb geo. height lat. grad. 21-day lead	0.089210
Gulf of Mexico SST anomaly	0.081849
NA mean 500 mb geo. height lat. grad. 21-day lead	0.079515
Relative humidity 28-day lead	0.077347

500 mb geo. height lat. grad. 24-day lead	0.076134
NAO 28-day lead	0.075246
California region	0.072062
500 mb geo. height lon. grad. 28-day lead	0.071524
Min. temp. 28-day lead	0.068009
NA mean 850 mb geo. height lon. grad. 24-day lead	0.067713
850 mb geo. height lon. grad. 24-day lead	0.065769
250 mb geo. height lat. grad. 24-day lead	0.062603
250 mb geo. height lon. grad. 24-day lead	0.061901
250 mb geo. height lon. grad. 21-day lead	0.056795
SOI	0.055560
MJO phase 21-day lead	0.054662
Austin 850 mb 21-day lead	0.054332
Daily precip. 28-day lead	0.052217
500 mb geo. height lat. grad. 21-day lead	0.052208
MJO amplitude 24-day lead	0.051944
Min. temp. 24-day lead	0.051546
NA mean 500 mb geo. height lat. grad. 24-day lead	0.050523
NA mean 250 mb geo. height lat. grad. 28-day lead	0.049487
Lower Colorado region	0.048683
NAO 21-day lead	0.047635
Austin 250 mb 28-day lead	0.047609
NAO 24-day lead	0.047261
NA mean 250 mb geo. height lon. grad. 21-day lead	0.045935
850 mb geo. height lat. grad. 24-day lead	0.044530
Austin 500 mb 21-day lead	0.044491
NA mean 500 mb geo. height lon. grad. 28-day lead	0.044122
500 mb geo. height lon. grad. 21-day lead	0.043450
NA mean 500 mb geo. height lon. grad. 24-day lead	0.043334
Daily precip. 24-day lead	0.042774

NA mean 850 mb geo. height lat. grad. 28-day lead	0.042581
Ohio region	0.041911
Austin 500 mb 28-day lead	0.041396
Arkansas-White-Red region	0.040911
Austin 850 mb 24-day lead	0.039321
850 mb geo. height lat. grad. 21-day lead	0.038024
NA mean 500 mb geo. height lon. grad. 21-day lead	0.037193
850 mb geo. height lon. grad. 21-day lead	0.036836
Wind speed 24-day lead	0.035513
NA mean 500 mb geo. height lat. grad. 28-day lead	0.035395
NA mean 250 mb geo. height lon. grad. 24-day lead	0.035135
Min. temp. 21-day lead	0.032755
Austin 850 mb 28-day lead	0.032710
500 mb geo. height lat. grad. 28-day lead	0.032695
850 mb geo. height lat. grad. 28-day lead	0.030618
Wind speed 28-day lead	0.026686
Wind speed 21-day lead	0.026078
NA mean 250 mb geo. height lon. grad. 28-day lead	0.025838
250 mb geo. height lon. grad. 28-day lead	0.023873
Max. temp. 28-day lead	0.022848
NA mean 850 mb geo. height lat. grad. 24-day lead	0.021930
Austin 250 mb 21-day lead	0.019894
Smoothed 85th percentile max. temp. climatology	0.019654
MJO phase 24-day lead	0.014217
Daily precip. 21-day lead	0.011749

Supplemental Table 1. Full SHAP scores from initial model performance before variable exclusion.